

Contrast-augmented Diffusion Model with Fine-grained Sequence Alignment for Markup-to-Image Generation

Guojin Zhong
College of Computer Science and
Electronic Engineering, Hunan
University
Changsha, China
gjzhong@hnu.edu.cn

Jin Yuan*
College of Computer Science and
Electronic Engineering, Hunan
University
Changsha, China
yuanjin@hnu.edu.cn

Pan Wang
College of Computer Science and
Electronic Engineering, Hunan
University
Changsha, China
wpanda@hnu.edu.cn

Kailun Yang
School of Robotics, Hunan University
Changsha, China
kailun.yang@hnu.edu.cn

Weili Guan
Monash University
Melbourne, Australia
honeyguan@gmail.com

Zhiyong Li*
School of Robotics, Hunan University
Changsha, China
zhiyong.li@hnu.edu.cn

ABSTRACT

The recently rising markup-to-image generation poses greater challenges as compared to natural image generation, due to its low tolerance for errors as well as the complex sequence and context correlations between markup and rendered image. This paper proposes a novel model named “Contrast-augmented Diffusion Model with Fine-grained Sequence Alignment” (FSA-CDM), which introduces contrastive positive/negative samples into the diffusion model to boost performance for markup-to-image generation. Technically, we design a fine-grained cross-modal alignment module to well explore the sequence similarity between the two modalities for learning robust feature representations. To improve the generalization ability, we propose a contrast-augmented diffusion model to explicitly explore positive and negative samples by maximizing a novel contrastive variational objective, which is mathematically inferred to provide a tighter bound for the model’s optimization. Moreover, the context-aware cross attention module is developed to capture the contextual information within markup language during the denoising process, yielding better noise prediction results. Extensive experiments are conducted on four benchmark datasets from different domains, and the experimental results demonstrate the effectiveness of the proposed components in FSA-CDM, significantly exceeding state-of-the-art performance by about 2% ~ 12% DTW improvements. The code will be released at <https://github.com/zgj77/FSACDM>.

CCS CONCEPTS

• **Computing methodologies** → *Artificial intelligence; Computer vision;*

*Corresponding author.

Permission to make digital or hard copies of all or part of this work for personal or classroom use is granted without fee provided that copies are not made or distributed for profit or commercial advantage and that copies bear this notice and the full citation on the first page. Copyrights for components of this work owned by others than the author(s) must be honored. Abstracting with credit is permitted. To copy otherwise, or republish, to post on servers or to redistribute to lists, requires prior specific permission and/or a fee. Request permissions from [permissions@acm.org](https://permissions.acm.org).

MM '23, October 29–November 3, 2023, Ottawa, ON, Canada.

© 2023 Copyright held by the owner/author(s). Publication rights licensed to ACM.

ACM ISBN 979-8-4007-0108-5/23/10...\$15.00

<https://doi.org/10.1145/XXXXXX.XXXXXX>

KEYWORDS

Markup-to-Image Generation; Diffusion Model; Contrastive Learning; Cross-attention; Text-to-Image Generation

ACM Reference Format:

Guojin Zhong, Jin Yuan, Pan Wang, Kailun Yang, Weili Guan, and Zhiyong Li. 2023. Contrast-augmented Diffusion Model with Fine-grained Sequence Alignment for Markup-to-Image Generation. In *Proceedings of the 31st ACM International Conference on Multimedia (MM '23)*, October 29–November 3, 2023, Ottawa, ON, Canada. ACM, New York, NY, USA, 10 pages. <https://doi.org/10.1145/XXXXXX.XXXXXX>

1 INTRODUCTION

The recent progress of generative models like Generative Adversarial Network (GAN) [37, 39] and Denoising Diffusion Probabilistic Model (DDPM) [17] has tremendously promoted the prosperity of text-to-image generation, which aims at generating a semantically matching image conditioned on a language description. Most existing image generation studies focus on generating natural images, where each ambiguous natural language expression may generate multiple semantically consistent images with diverse appearances.

As a comparison, Deng *et al.* [8] recently proposed a novel text-to-image task called “markup-to-image”, which aims at mapping a structured markup description like mathematical formulas, HTML simple tables, music notations, and chemical molecules (see Figure 1 (a)), into an exact image, which could precisely express the corresponding markup language. Different from natural image generation, markup-to-image task has known ground truth to facilitate models’ evaluation. Moreover, the compositional nature of markup language requires a deeper exploration of relational properties, which poses greater challenges for this task.

Benefiting from advances in Diffusion Models (DMs) for image generation [32], Deng *et al.* first designed a DM with scheduled sampling for markup-to-image generation. This approach attempts to alleviate the exposure bias problem in DMs, where a model is never exposed to incorrectly generated tokens during the training but frequently faces these errors in the inference phase. Despite the success, it still has the following drawbacks when applied in markup-to-image generation: First, it does not explore the fine-grained temporal alignment relationship between a markup language description and the corresponding rendered image, which

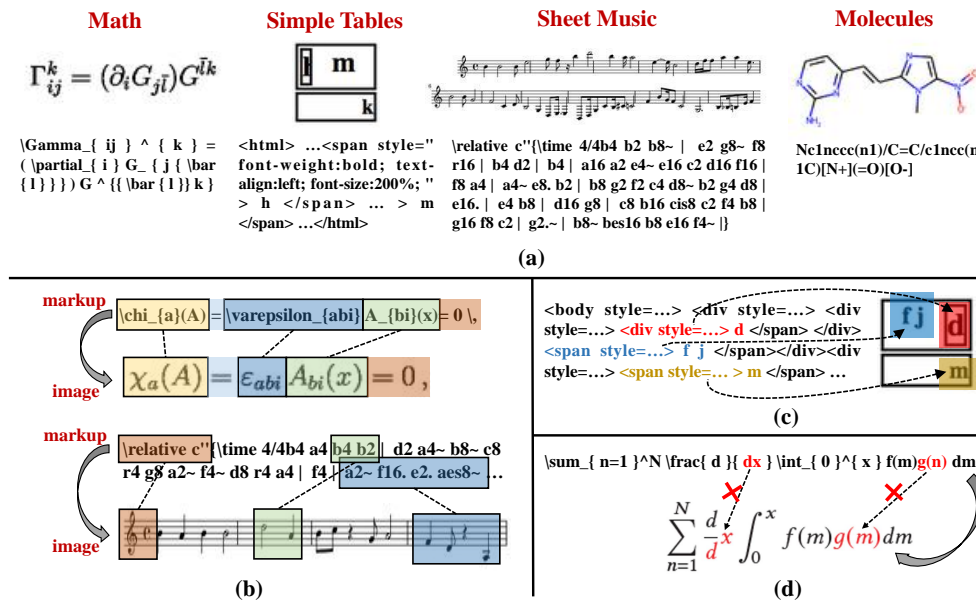


Figure 1: Several examples to illustrate the datasets of markup-to-image (Sub-figure (a)) as well as its characteristics, including the sequence relationship between markups and images (Sub-figure (b)), the contextual correlation within a markup description (Sub-figure (c)), and the low tolerance for character errors (Sub-figure (d)).

is widely present in the data of this task (see Figure 1 (b)); Second, there is strong compositional nature of markup language, and capturing the contextual correlation within a markup description is crucial for a deep understanding (see Figure 1 (c)); Third, markup-to-image has a low tolerance for errors, and even a small symbol error may cause a complete semantic bias (see Figure 1 (d)). Thus, using a single image construction process in DMs without positive/negative contrastive feedback is not conducive to improving the model’s generalization.

Towards this end, this paper proposes a novel Contrast-augmented Diffusion Model with Fine-grained Sequence Alignment (FSA-CDM), which exposes the model to both positive and negative samples with powerful feature learning for markup-to-image generation. Specifically, given a pair of image and markup inputs, we first encode them into a sequence of visual and language tokens, respectively. Then, we employ Bi-LSTM to capture the contextual relationship among visual tokens and design a fine-grained cross-modal alignment module to well align each visual token with the corresponding textual token sequence by sequence. On this basis, we propose a contrast-augmented diffusion model for markup image generation. Different from [8] only receiving a single sample for construction, FSA-CDM receives a to-be-constructed sample with several contrastive positive/negative samples to augment the model’s training. We mathematically design a contrastive variational objective integrating both positive and negative samples and infer a tighter bound for optimization. By contrastively exploring multiple samples, FSA-CDM could better improve the model’s generalization ability as well as reduce prediction errors. Furthermore, we design a Context-aware Cross Attention Module (CCAM) to replace the traditional cross attention during the denoising process.

CCAM constructs a relationship matrix from visual features to explore the complex contextual relationship among markup inputs, and thus could better predict noise for image construction.

Extensive experiments are carried out on all four benchmark datasets from different domains. Our FSA-CDM presents high-quality image generation and significantly outperforms state-of-the-art (SOTA) methods on all the benchmark datasets. Our contributions are summarized as follows:

- We propose a fine-grained sequence alignment module to align markup language and its rendered image at the sequence level, thereby learning robust uni-modal representations to support markup-to-image generation.
- We propose a contrast-augmented diffusion model that explicitly introduces positive and negative samples by using contrastive learning. A novel contrastive variational objective is mathematically inferred to achieve a tighter bound for variational evidence, improving the model’s generalization ability as well as alleviating the exposure bias problem.
- We design a context-aware cross attention module for noise prediction during the denoising process. CCAM constructs a relationship matrix between characters from visual features to guide the contextual information capturing among markup language, yielding accurate noise prediction.

2 RELATED WORK

2.1 Text-to-Image Generation

The early text-to-image generation adopts Generative Adversarial Networks (GAN) [15], which was first proposed by Reed *et al.* [31]. On this basis, a variety of studies on GANs have been proposed

to improve the quality of image generation via progressive refinement [44, 45], cross-modal attention [34, 41, 43] as well as semantic modeling [6, 26, 35]. Another text-to-image generation paradigm adopts VQ-VAE [30, 36] to generate discrete image markers from text cues. Imposing VQ-VAE, transformer-based approaches like DALLE [29] and CogView [12] could effectively generate images from text prompts but suffer from the limitations of autoregressive models with one-way bias and cumulative prediction errors [27].

Diffusion model (DM) [17, 23] is a recently rising approach in text-to-image generation, which attempts to add noises into an image step by step followed by the denoising process to reconstruct the image. Compared to GAN-based methods, DMs are free of training instability and mode collapse [10], and thus demonstrate impressive performance for image generation [28, 33]. For instance, Gu *et al.* proposed VQ-Diffusion [16] based on VQ-VAE to eliminate the one-way bias and cumulative prediction errors, yielding better image quality. Liu *et al.* [22] proposed a composable DM to solve the semantic deficiency, where an image is generated by a set of diffusion models, each modeling a component of the image. Benny *et al.* [2] proposed a dynamic dual-output DM to address the problem of poor-quality images when the number of iterations is low. Besides, several studies aimed at improving the understanding of text inputs. For instance, Xu *et al.* [40] proposed a method combining CLIP, which uses high-quality images generated by a pre-trained text DM for all-view segmentation. Zhao *et al.* further proposed MagicFusion [46] to fuse multiple text-guided DMs to improve image quality. Gao *et al.* proposed a Masked Diffusion Transformer [14], which can reconstruct the complete information of an image from an incomplete contextual input. More advanced researches on DMs for image generation include DMs on semi-supervised learning [47], DMs on attention mechanism [4], *etc.* Recently, Deng *et al.* [8] first proposed a novel image generation task named markup-to-image by DM. Different from natural image generation with flexible interpretations of text prompts, markup-to-image generation aims to generate an exact image under a unique interpretation of a given markup prompt and has a low tolerance for symbol errors, which greatly increases the technical challenges.

2.2 Contrastive Learning in Generative Model

Contrastive learning is a powerful self-supervised representation learning [5] approach that has been used in generative models. For instance, Kang *et al.* proposed ContraGAN [19] to consider the relationship of multiple image embeddings as well as the data-to-class relationship by using a conditional contrast loss. Yang *et al.* proposed DiscoFaceGAN [9] to add contrastive learning to face generation to facilitate untangling, allowing precise control of face attributes. Ye *et al.* [42] proposed a contrastive learning method to learn consistent textual representations of captions corresponding to the same image, thereby enhancing the quality and semantic consistency of synthetic images. In addition, Parmar *et al.* indicated that contrastive learning can be combined with metric learning to improve VAE, solving the instance-level fidelity between input and reconstruction in the induced feature space. ContrastVAE [38] creates two views for input data to alleviate the uncertainty and sparsity issues, thereby improving the generalization ability of VAE.

For diffusion models, Ouyang *et al.* [24] found that enhancing distinguishability was important and thus adopted the contrastive loss to guide the diffusion model. In order to improve the connection between input and output, Zhu *et al.* [48] designed a conditional discrete contrastive diffusion loss, which directly incorporates negative samples into the model’s training for optimizing the evidence lower bound. Although the above methods have achieved good results in image generation, they simply introduce the contrastive loss into DMs in a separate learning pattern or only incorporate negative samples to DMs to optimize conventional variational objectives, which has limited learning capability on image generation.

Beyond the previous studies, this work explicitly incorporates both positive and negative samples into DM for better optimizing variational objectives to provide a tighter bound for evidence, thereby improving discrimination and generalization performance for markup-to-image generation. Moreover, our approach first explores sequence and context relationships for markup-to-image generation, and thus could better capture the correlations between visual and textual features for performance improvement.

3 METHOD

In this section, we first present the definition of markup-to-image generation, and then describe our Contrast-augmented Diffusion Model with Fine-grained Sequence Alignment (FSA-CDM). The overall framework of FSA-CDM is illustrated in Figure 2, which consists of two parts: an image and a markup encoder with fine-grained sequence alignment to extract robust uni-modal representations, and a contrast-augmented diffusion model with a context-aware attention module to accurately generate rendered images.

3.1 Task Definition

Given a markup language $x \in \mathcal{X}$ and its corresponding rendered image $y \in \mathcal{Y}$, the goal of markup-to-image is to establish a model $f_\theta : \mathcal{X} \rightarrow \mathcal{Y}$ to approximate the true mapping $f : \mathcal{X} \rightarrow \mathcal{Y}$ trained on supervised data. Specifically, the markup language we focus on includes latex formulas, HTML codes, musical notations, and chemical molecular sequences. Different from the natural image synthesis benchmarks, the layout of rendered images corresponding to the markups is more discrete, which increases the difficulty of feature extraction. Besides, a rendered image also has a long-term symbol dependency, and thus the accumulation of local errors can lead to information deviation conveyed by the entire image.

3.2 Input Representation

As mentioned in section 3.1, the input of markup-to-image is a set of paired markups and rendered images, denoted as (\mathbf{X}, \mathbf{Y}) . For a markup sequence \mathbf{x} , the pre-trained markup language model [7, 13] is employed as an encoder to obtain its embedding representation $\mathbf{t} \in \mathbb{R}^{N \times D}$, where N and D are the number of tokens and the dimension of each token, respectively. Following the previous work [8], we adopt ResNet to extract visual features $\mathbf{v} \in \mathbb{R}^{C \times H \times W}$ for a rendered image \mathbf{y} , where C , H , and W are the channel, height, and width of \mathbf{v} , respectively. Since rendered images have a sequential structure with rich contextual information, we propose to progressively optimize visual features and align them with the corresponding markup embeddings to learn robust uni-modal representations.

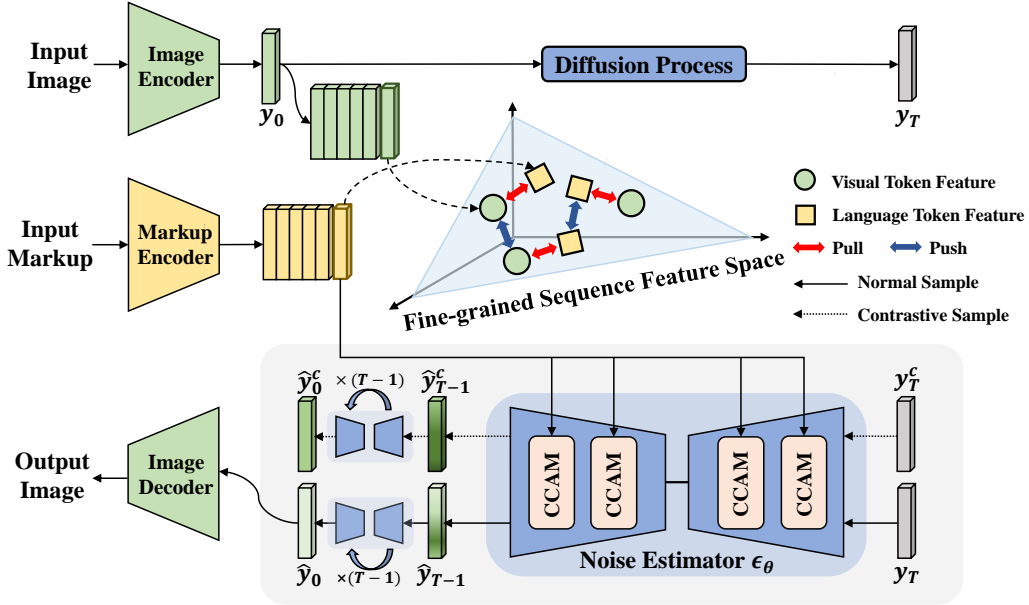


Figure 2: The framework of FSA-CDM, which consists of an image and a markup encoder with fine-grained cross-modal alignment, and a contrast-augmented diffusion model containing several CCAMs, where y_0 , y_T , \hat{y}_t and \hat{y}_t^c denote original samples, full-noise samples, denoising samples, and contrast-augmented positive/negative samples, respectively.

Sequential Visual Feature Capturing. We first use a *convolution + map-to-sequence* operation [1] to convert \mathbf{v} into a sequence of visual tokens $\mathbf{v}^s = (v^s_1, v^s_2, \dots, v^s_M) \in \mathbb{R}^{M \times D}$, where each token corresponds to a receptive field in \mathbf{y} and the number of tokens M depends on the width of \mathbf{y} . Afterward, \mathbf{v}^s is fed into a bidirectional LSTM (Bi-LSTM) [20] to capture the contextual information, allowing each token to distinguish itself from its semantic context as well as capture the long-term symbol dependency. Finally, we refine \mathbf{v}^s by concatenating the hidden states $\mathbf{h} = (h_1, h_2, \dots, h_M) \in \mathbb{R}^{M \times D}$ output by Bi-LSTM, as suggested in [21].

Fine-grained Cross-modal Alignment. Considering that a pair of markup and rendered image inputs sequentially convey consistent semantics, it is important to explicitly mine the sequence-similarity between them. Therefore, we propose a fine-grained alignment pattern at the sequence level as illustrated in Figure 2, aiming at learning more robust uni-modal representations.

Specifically, a cross-attention module $CAM(\cdot, \cdot, \cdot)$ [18] is first employed to capture the receptive field-to-token relevance between the input image and markup:

$$\mathbf{c} = CAM(\mathbf{t}, \mathbf{v}^s, \mathbf{v}^s), \quad (1)$$

where $\mathbf{c} \in \mathbb{R}^{N \times D}$ is an evolved feature with the same length as \mathbf{t} , and \mathbf{t} , \mathbf{v}^s and \mathbf{v}^s are the query, key, and value matrices, respectively. Then, we define a fine-grained alignment loss to optimize the correlation between the two modalities, where c_i is encouraged to be similar to \mathbf{t}_i with the same index and dissimilar to \mathbf{t}_j with different indexes ($i \neq j$). As cosine similarity $\cos(\cdot, \cdot)$ is employed to measure the sequence-similarity, the fine-grained cross-modal alignment

loss \mathcal{L}_{fa} can be formulated as:

$$\mathcal{L}_{fa} = \frac{1}{N} \sum_{i=1}^N [1 - \cos(c_i, \mathbf{t}_i)] + \frac{1}{N-1} \sum_{j=1, j \neq i}^N \cos(c_i \cdot \mathbf{t}_j). \quad (2)$$

The optimization of \mathcal{L}_{fa} allows us to better learn the inter-modal sequence similarity between rendered images and markups, thereby obtaining more robust uni-modal representations.

3.3 Contrast-augmented Diffusion Model

Given a variable y_0 , most of the diffusion models (DMs) maximize the evidence lower bound (ELBO) of $\log p(y_0)$ on the Markov chain $q(y_1, \dots, y_T | y_0) = \sum_{t=1}^T q(y_t | y_{t-1})$:

$$\begin{aligned} \text{maximize } \log(y_0) &\geq \mathbb{E}_q \log \frac{p(y_{0:T})}{q(y_{1:T} | y_0)} \\ &= \mathbb{E}_q [\log p(y_0 | y_1) - D_{KL}(q(y_T | y_0) || p(y_T))] \\ &\quad - \sum_{t=1}^T D_{KL}(q(y_{t-1} | y_t, y_0) || p(y_{t-1} | y_t)) \\ &= \mathcal{L}_{elbo}(y_0), \end{aligned} \quad (3)$$

where q denotes the probabilistic distribution of real data, and p is an approximate probability distribution of q . $D_{KL}(\cdot || \cdot)$ is Kullback-Leibler Divergence, which is widely used to measure the difference between two distributions. On this basis, our approach introduces contrastive learning into the diffusion model, which exposes the model to both positive and negative samples to improve the generalization ability as well as alleviate the exposure bias problem. Specifically, we explicitly consider the expected states of positive

sample y'_0 and negative sample \bar{y}_0 based on the original variational inference, which maximizes the log-likelihood of y'_0 as well as minimizes the log-likelihood of \bar{y}_0 , as shown in the following objective:

$$\text{maximize } \log p(y_0, y'_0) - \lambda \log p(\bar{y}_0), \quad (4)$$

where λ is a balanced weight. It is very difficult to directly solve Equation 4, and thus we optimize it to maximize the variational lower bound as follows:

$$\begin{aligned} & \log p(y_0, y'_0) - \lambda \log p(\bar{y}_0) \\ & \geq \mathcal{L}_{elbo}(y_0, y'_0) - \lambda \mathcal{L}_{elbo}(\bar{y}_0), \end{aligned} \quad (5)$$

where $elbo$ represents the evidence upper bound. Specifically, we use mild augmentation [1] and same-batch sampling strategies [5] to create a positive sample y'_0 and several negative samples \bar{y}_0 for each y_0 , respectively. Below, we will describe the process of solving these two log-likelihood boundaries.

ELBO of Positive Log-likelihood. Since y'_0 is another view of y_0 , we propose to model them in a logarithmic joint likelihood $\log p(y_0, y'_0)$ and take into account y_t generated at each step t during the diffusion process (see Appendix A.1 for details):

$$\begin{aligned} \log p(y_0, y'_0) &= \log \int_{y'_1, \dots, y'_{t-1}} \int_{y_1, \dots, y_{t-1}} p(y_0, y_t, y'_0, y'_t) dy_t dy'_t \\ &\geq \mathbb{E}_{q(y_t, y'_t | y_0, y'_0)} \log \left[\frac{p(y_0, y_t, y'_0, y'_t)}{q(y_t, y'_t | y_0, y'_0)} \right] \\ &= \mathcal{L}_{elbo}(y_0) + \mathcal{L}_{elbo}(y'_0) + \mathbb{E}_{y_t, y'_t} [MI(y_t, y'_t)], \end{aligned} \quad (6)$$

where $MI(\cdot, \cdot)$ is mutual information [25]. From Equation 6, it can be seen that one of the goals is to maximize the mutual information between y_t and y'_t , which enables the model to emphasize the similarity relationships between samples. By training on these relationships, our model learns to better capture the essential features of similar samples, thereby improving generalization ability.

EUBO of Negative Log-likelihood. EUBO has favorable properties: it has a mass covering effect advantageous in the approximation of the posterior, and thus provides a tighter bound for the variational evidence. Equation. 5 can be optimized (see Appendix A.2 for details) by using the method [11]:

$$\begin{aligned} \log p(\bar{y}_0) &\leq CUBO_{\chi^2} = \frac{1}{2} \log \mathbb{E}_{q(\bar{y}_t)} \left[\left(\frac{p(\bar{y}_0, \bar{y}_t)}{q(\bar{y}_t)} \right)^2 \right] \\ &\triangleq \exp(2CUBO_{\chi^2}) = \mathbb{E}_{q(\bar{y}_t | \bar{y}_0)} \left[\left(\frac{p(\bar{y}_0, \bar{y}_t)}{q(\bar{y}_t | \bar{y}_0)} \right)^2 \right] \\ &= \mathbb{E}_{q(\bar{y}_t | \bar{y}_0)} \left(e^{2 \log \frac{p(\bar{y}_0, \bar{y}_t)}{q(\bar{y}_t | \bar{y}_0)}} \right) = e^{2 \mathcal{L}_{elbo}(\bar{y}_0)}. \end{aligned} \quad (7)$$

Different from [48] only using negative samples to increase the lower bound, our model explicitly considers the impact of both positive and negative logarithmic likelihoods by placing evidence between tighter upper and lower bounds, resulting in better variational inference for performance improvement.

Training. We jointly train all the components in FSA-CDM, and the final loss function is expressed as:

$$\begin{aligned} \mathcal{L}_{FSA-CDM} &= \beta \mathcal{L}_{fa} - \mathcal{L}_{elbo}(y_0) - \mathcal{L}_{elbo}(y'_0) \\ &\quad + \lambda e^{2 \mathcal{L}_{elbo}(\bar{y}_0)} - \mathbb{E}_{y_t, y'_t} [MI(y_t, y'_t)], \end{aligned} \quad (8)$$

where β is the weight of fine-grained sequence alignment loss in Equation. 2. For the mutual information term, we adopt the

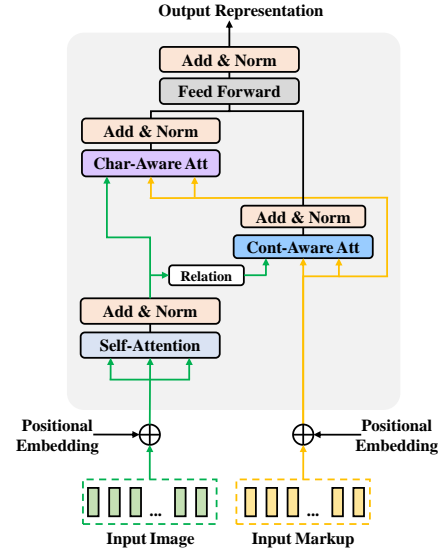


Figure 3: Context-aware Cross Attention Module (CCAM), which consists of a self-attention module, a character-aware attention module, and a context-aware attention module. The green and yellow paths represent visual and markup features, respectively.

contrastive loss \mathcal{L}_{cl} to efficiently approximate it as follows:

$$\mathcal{L}_{cl} = \log \frac{\exp(y_t^T \cdot y'_t / \tau)}{\sum \exp(y_t^T \cdot \bar{y}_t / \tau)}, \quad (9)$$

where τ is a temperature parameter. As a result, Equation. 8 can be rewritten as:

$$\mathcal{L}_{FSA-CDM} = \beta \mathcal{L}_{fa} - \mathcal{L}_{elbo}(y_0) - \mathcal{L}_{elbo}(y'_0) + \lambda e^{2 \mathcal{L}_{elbo}(\bar{y}_0)} - \mathcal{L}_{cl}. \quad (10)$$

3.4 Context-aware Cross Attention Module

The information conveyed by an input markup and its corresponding image mainly includes characters and their contextual correlations. Motivated by this, we design a Context-aware Cross Attention Module (CCAM) to better fuse visual and markup representations during the denoising process.

The structure of CCAM is shown in Figure 3, which mainly consists of three parts: self-attention (SA), character-aware attention (ChA), and context-aware attention (CoA). The SA is used to capture the internal dependencies between elements of visual features, and its output v^{sa} is fed into parallel ChA and CoA. In ChA, we transform v^{sa} into the queries $Q_{ca} \in \mathbb{R}^{N \times d_q}$, and markup representations t into keys $K_{ca} \in \mathbb{R}^{N \times d_k}$ and values $V_{ca} \in \mathbb{R}^{N \times d_v}$. The intuition is that the content of a rendered image is discrete, and thus we need to suppress unrelated parts in v^{sa} and accurately construct connections between referring characters in v^{sa} and the corresponding entities in t . Therefore, we perform ChA as:

$$ChA(Q_{ca}, K_{ca}, V_{ca}) = \text{softmax} \left(\frac{Q_{ca} K_{ca}^T}{\sqrt{d_k}} \right) V_{ca}. \quad (11)$$

Besides the exploration of characters, it is also necessary to have a deep understanding of the contextual information formed among characters. For instance, “ $\frac{1}{2}$ ” is often followed by the numerator and denominator strings in order, which could help the model better understand the contextual semantics. For this purpose, we develop the CoA, which is combined with ChA to finely learn multi-modal features. First, we obtain a relation matrix $\mathcal{R} = r_{ij}$ based on \mathbf{v}^{sa} by using the approach proposed in [3] with a low computational overhead, where r_{ij} describes the contextual relationship between image region i and region j . We linearly project (denoted as $\Psi(\cdot)$) the relation matrix \mathcal{R} as queries, denoted as $Q_{cu} \in \mathbb{R}^{N \times d_q}$:

$$\mathbf{v} \rightarrow \mathcal{R} = r_{ij}, Q_{cu} = \Psi(\mathcal{R}). \quad (12)$$

Afterward, we concatenate (denoted as $\Phi(\cdot, \cdot)$) the visual and markup features at the sequence level and send them into two different linear layers to obtain the sequence memory keys $K_{cu} \in \mathbb{R}^{(N+HW) \times d_k}$ and values $V_{cu} \in \mathbb{R}^{(N+HW) \times d_v}$, which contain potential cross-modal semantics:

$$K_{cu} = \Psi(\Phi(\mathbf{v}, \mathbf{t})), V_{cu} = \Psi(\Phi(\mathbf{v}, \mathbf{t})). \quad (13)$$

Finally, we take the cross-attention operation to capture the intra- and inter-modality semantic relationship, to help the model better understand contextual information:

$$\text{CoA}(Q_{cu}, K_{cu}, V_{cu}) = \text{softmax}\left(\frac{Q_{cu}K_{cu}^T}{\sqrt{d_k}}\right)V_{cu}. \quad (14)$$

Compared to the traditional cross-attention used in the denoising process, our approach could simultaneously capture notable characters and the potential contextual information among them, and thus could better output noises to support image construction.

4 EXPERIMENTS

4.1 Datasets

We conduct experiments on datasets from four domains:

Math is a large collection of real-world mathematical expressions written in LaTeX markups and their rendered images. There are a total of 55,033 training, 6,072 validation, and 1,024 testing text-image pairs, where the image size is 64×320 and the input markup contains 113 characters on average.

Simple Tables were collected based on the 100k synthesized HTML snippets and the corresponding rendered webpage images. There are 80,000 training, 10,000 validation, and 1,024 testing pairs, where the image size is 64×64 with an average of 481 characters in markup text.

Sheet Music adopts LilyPond files as its markup language, and generates 32,880 markup-image pairs, including 30,902 for training, 989 for validation, and 988 for testing. The image size is 192×448 with an average of 240 characters in markup text.

Molecule from the chemistry domain contains 19,925 2D molecules images specified by SMILES strings. It is divided into 17,925 training, 1,000 validation, and 1,000 testing samples. Different from the other three datasets, the rendered image in Molecules is colored with a size of 128×128 and an average length of 30 in markup text.

4.2 Implementation Details

Experimental Settings. Following [8], we initiate the markup encoder with GPT-Neo-175M [13] for Math, Simple Tables, and Sheet Music datasets and ChemBert-77M-MLM [7] for Molecules dataset. For input images, we build a lightweight ResNet as the image encoder. The relevant settings of our diffusion scheduler refer to the HuggingFACE diffusers library¹, where the noise estimator is a U-Net with five CCAMs and eight conventional cross-attention layers. We use mild augmentation strategy [1] to create a positive sample that maintains semantic consistency for each training sample. And five negative samples are sampled from the same batch [5], which have different semantics from the positive sample. The weights λ and β are set to 0.005 and 0.02, respectively. We set the batch sizes for Math, Simple Tables, Music and Molecules are 16, 24, 8 and 16, respectively, and we train all models for 100 epochs using the Adam optimizer with the learning rate 0.0001 on 4 Nvidia RTX A6000 with 48 GPU VRAM. The learning rate is decreased by the cosine decay strategy with 500 warmup steps.

Metrics. For the markup-to-image task, the generated image should be consistent with the ground truth image at the pixel level, which is different from other popular image-generation tasks. Therefore, we adopt Dynamic Time Warping (DTW) and Root Squared Mean Error (RMSE) as our main evaluation metrics following [8]. RMSE compares two images at the pixel level, and it penalizes the generated image with smaller character offsets, even if it is semantically equivalent to the ground truth image. DTW calculates pixel-level similarity by treating an image as time series through binarization and allows minor offsets of the generated image, which fits the markup-to-image task. Structural similarity index measure (SSIM), peak signal-to-noise ratio (PSNR), erreur relative globale adimensionnelle de synthèse (ERGAS), and relative average spectral error (RASE) serve as supplements for the above two main metrics to report performance more comprehensively.

4.3 Comparison with state-of-the-art methods

We compare the proposed method with several SOTA methods, including XMC-GAN [43], SS-DM [8], and CDCD [48] on Math, Simple Tables, Sheet Music, and Molecules datasets. All the approaches except SS-DM are replicated by using the optimization parameter settings.

Quantitative Analysis. We calculate six evaluation metrics mentioned above and show the results in Table 1. Benefitting from the stable training of the diffusion model, SS-DM achieves better performance as compared to XMC-GAN, and CDCD further improves the performance due to the introduction of negative samples by using contrastive learning during the denoising process. Comparatively, our FSA-CDM achieves the best performance with a significant improvement on all the metrics because FSA-CDM introduces a robust feature learning module and contrastive positive and negative samples for the diffusion model, generating stronger generalization ability. In addition, we discover that the DTW improvement by FSA-CDM is greater than the RMSE improvement. This is because DTW is a relaxed pixel-level similarity and is consistent with our encoding process, which divides a text-image pair into a sequence of visual and textual tokens with the alignment on the

¹<https://github.com/huggingface/diffusers>

Table 1: Evaluation results of four advanced approaches on four datasets, where DTW and RMSE are the main evaluation metrics, supplemented by SSIM, PSNR, ERGAS, and RASE. “Params” and “Throughput” denote the parameter complexity (M) and inference speed (seconds/Img), respectively, where all DMs perform 1000 denoising steps for inference.

Dataset	Approach	Main Metrics			Complimentary			Inference	
		DTW↓	RMSE↓	SSIM↑	PSNR↑	ERGAS↓	RASE↓	Params	Throughput
Math	XMC-GAN	20.05	38.56	0.77	16.93	2367.48	592.55	174	<1
	SS-DM	18.81	37.19	0.79	17.25	2247.41	561.85	209	48
	CDCD	17.98	36.47	0.79	17.04	2164.14	550.31	195	44
	FSA-CDM	15.76	34.52	0.81	18.14	1996.54	496.23	253	53
	Improvements	+12.34%	+5.35%	+2.53%	+6.46%	+7.74%	+9.83%	-	-
Simple Tables	XMC-GAN	6.15	23.08	0.90	38.14	2523.83	657.46	174	<1
	SS-DM	5.64	21.11	0.93	40.20	2285.83	571.46	209	46
	CDCD	5.47	20.63	0.94	41.03	2176.21	557.76	195	43
	FSA-CDM	5.03	19.78	0.95	42.35	2024.16	508.14	253	51
	Improvements	+8.04%	+4.12%	+1.06%	+3.22%	+6.99%	+8.90%	-	-
Sheet Music	XMC-GAN	80.77	45.21	0.67	15.14	3036.52	761.09	174	<1
	SS-DM	79.76	44.70	0.68	15.20	2978.36	744.59	209	137
	CDCD	78.93	44.26	0.69	15.35	2937.57	733.05	195	127
	FSA-CDM	76.79	43.41	0.71	15.73	2866.71	707.24	253	151
	Improvements	+2.71%	+1.92%	+2.90%	+2.48%	+2.41%	+3.52%	-	-
Molecules	XMC-GAN	25.04	38.22	0.60	16.60	2496.33	623.58	174	<1
	SS-DM	24.80	37.92	0.61	16.69	2467.16	616.79	209	126
	CDCD	24.31	36.86	0.63	16.87	2415.08	600.32	195	117
	FSA-CDM	23.69	36.14	0.63	17.06	2386.35	574.57	253	139
	Improvements	+2.55%	+1.95%	+0.00%	+1.12%	+1.19%	+4.29%	-	-

token level. What is more, the improvements in the Math and Tables domains are more significant than that in Music and Molecules since Music and Molecules have a long dependence chain of symbols, which is too difficult to be captured. Despite the success, DM-based approaches are much slower than GAN-based approaches like XMC-GAN since they require multiple denoising steps. Our FSA-CDM is inferior to CDCD and SS-DM in terms of parameters and inference speed. The increase in model parameters stems from the feature extraction module and CCAM, and the inference time is mainly affected by CCAM during the denoising process. The introduction of contrastive samples has no effect on the inference time. Fortunately, the delay is tolerable and can be alleviated by reducing the denoising steps at the expense of accuracy [16].

Qualitative Analysis. Figure 4 presents several markup images generated by SOTA methods and the corresponding ground truth, qualitatively comparing the performance of markup-to-image generation. All the methods exhibit different adaptations to the four domains with varying degrees of difficulty. Specifically, these methods perform well in math and simple tables domain, and our FSA-CDM achieves the best visual effects for human eyes. For the music domain, due to the bottleneck of the long dependence chain of symbols from left to right, it is difficult for the model to maintain accuracy after generating the top few symbols due to the limited number of denoising steps. The molecules image generated by FSA-CDM is the closest to the ground truth, considering the non-uniqueness of the molecules’ layout and orientation.

4.4 Ablation Study

This experiment verifies the effectiveness of the proposed three components, including the fine-grained sequence module (FSA.), the contrast-augmented diffusion model (Con-aug.), and the context-aware cross attention module (CCAM.). Table 2 demonstrates the comparison results on four benchmarks, where we remove the

components of FSA., Con-aug. and CCAM. as our baseline model. From the table, we can draw the following conclusions: First, the introduction of FSA. decreases DTW by 3.03%, 2.59%, 1.47%, and 1.03% than the baseline model on Math, Simple Tables, Sheet Music, and Molecules, respectively, which indicates that the sequence alignment capturing between markups and images by our encoding is effective, yielding robust uni-modal representations at a fine-grained level. Second, compared with the baseline network, we explicitly introduce contrastive positive and negative samples in the denoising process, bringing 12.02%, 8.80%, 2.73%, and 2.93% DTW improvements on four benchmarks, respectively. This superior performance gain proves that contrastive samples can encourage the diffusion model to capture more similar and discriminative information during training to improve its generalization ability. Moreover, when Con-aug. is combined with FSA., it can achieve an average DTW improvement of 8.84% compared to the baseline model. Third, benefiting from a deeper exploration of character and contextual correlations, the proposed CCAM achieves 6.95%, 6.21%, 2.05%, and 1.77% DTW improvements, respectively. Finally, our approach combining the three proposed components decreases the average DTW and RMSE by 10.21% and 6.35%, which is significantly better than the baseline model.

4.5 Analysis of Contrastive Variational Loss

The balanced weight λ in contrastive variational loss is a sensitive parameter. To show how λ affects the performance of markup-to-image generation, we set different values of λ to observe the performance change on Math and Molecules datasets as shown in Table 3. When λ is equal to 0, i.e. ignoring the optimization of the variational evidence bound by negative samples, we can observe that the performance is the worst. As λ increases from 0 to 0.005, the performance is consistently improved, which proves the effectiveness of negative variational loss since negative samples can

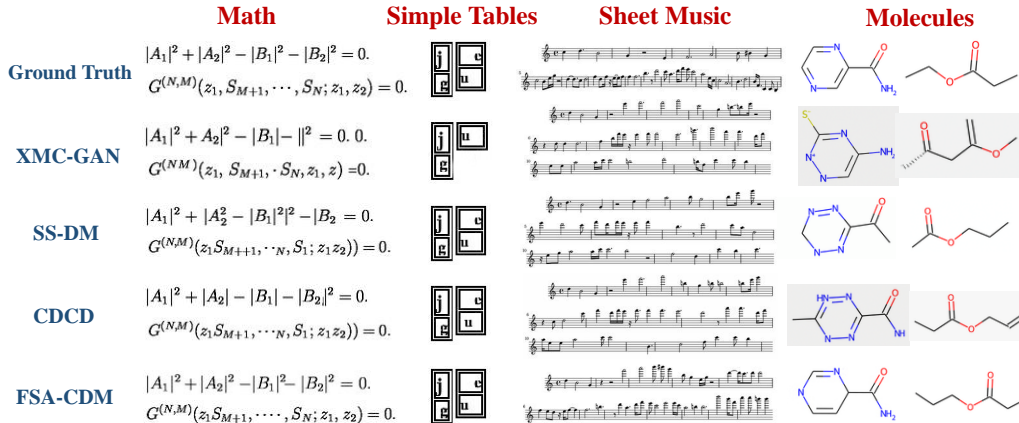


Figure 4: Qualitative results on four datasets. The columns from left to right are Math and Simple Tables, Sheet Music, and Molecules, respectively. And the rows from top to bottom are ground truth, XMC-GAN, SS-DM, CDCD, and FSA-CDM, respectively.

Table 2: Evaluation results of ablation studies on four datasets.

Dataset	Different Setting			Main Metrics	
	FSA.	Con-aug.	CCAM	DTW↓	RMSE↓
Math	-	-	-	19.12	37.54
	✓	-	-	18.54	36.85
	-	✓	-	16.82	35.47
	-	-	✓	17.79	36.44
	✓	✓	-	16.23	34.96
	✓	✓	✓	15.76	34.52
Simple Tables	-	-	-	5.79	21.34
	✓	-	-	5.64	20.96
	-	✓	-	5.28	20.29
	-	-	✓	5.43	20.67
	✓	✓	-	5.11	19.96
	✓	✓	✓	5.03	19.78
Sheet Music	-	-	-	79.85	44.92
	✓	-	-	78.68	44.35
	-	✓	-	77.67	43.79
	-	-	✓	78.21	44.07
	✓	✓	-	77.17	43.58
	✓	✓	✓	76.79	43.41
Molecules	-	-	-	24.91	38.05
	✓	-	-	24.67	37.64
	-	✓	-	24.18	36.83
	-	-	✓	24.47	37.26
	✓	✓	-	23.85	36.42
	✓	✓	✓	23.69	36.14

provide dissimilar information for our model to learn differential features between positive and negative samples, thereby improving generalization ability. However, the further increase of λ would lead to a performance drop because a too-large value of λ would overshadow the utility of positive samples, which are the dominant elements in the denoising process.

Table 3: Evaluation results of contrastive variational loss with different weights λ on Math and Molecules datasets.

λ	0	0.002	0.005	0.01	0.02
DTW on Math	16.34	16.07	15.76	15.94	16.29
RMSE on Math	35.18	34.90	34.52	34.77	35.05
DTW on Molecules	24.38	24.02	23.69	23.76	24.06
RMSE on Molecules	37.21	36.65	36.14	36.32	36.68

5 CONCLUSIONS

In this work, we propose a novel “Contrast-augmented Diffusion Model with Fine-grained Sequence Alignment” (FSA-CDM) for markup-to-image generation. Beyond the existing diffusion models, our approach first incorporates positive and negative samples with a novel contrastive variational objective to offer a tighter bound to improve the model’s generalization ability, which generates important theoretical values. In addition, different from natural image generation, our approach considers the characteristics of markup images, including the sequence correlations by using the fine-grained sequence alignment and the complex context by designing the context-aware cross attention module. Extensive experiments on four benchmark datasets confirm the effectiveness of the proposed approach. However, it still has limitations in terms of long dependency chains and inference speed. In future work, we will further explore these issues and attempt to apply the proposed theory to other generation tasks.

ACKNOWLEDGMENTS

This work was supported by the National Natural Science Foundation of China (No. 62272157, No. U21A20518, and No. 61976086) and the Natural Science Foundation of Changsha (No. kq2202177).

REFERENCES

- [1] Aviad Aberdam, Ron Litman, Shahar Tsiper, Oron Anschel, Ron Slossberg, Shai Mazor, R Manmatha, and Pietro Perona. 2021. Sequence-to-sequence contrastive learning for text recognition. In *Proceedings of the IEEE/CVF Conference on Computer Vision and Pattern Recognition (CVPR)*.
- [2] Yaniv Benny and Lior Wolf. 2022. Dynamic Dual-Output Diffusion Models. In *Proceedings of the IEEE/CVF Conference on Computer Vision and Pattern Recognition (CVPR)*.
- [3] Jie Cao, Shengsheng Qian, Huaiwen Zhang, Quan Fang, and Changsheng Xu. 2021. Global relation-aware attention network for image-text retrieval. In *Proceedings of the International Conference on Multimedia Retrieval (ICMR)*.
- [4] Hila Chefer, Yuval Alaluf, Yael Vinker, Lior Wolf, and Daniel Cohen-Or. 2023. Attend-and-Excite: Attention-Based Semantic Guidance for Text-to-Image Diffusion Models. In *Proceedings of the IEEE/CVF Conference on Computer Vision and Pattern Recognition (CVPR)*.
- [5] Ting Chen, Simon Kornblith, Mohammad Norouzi, and Geoffrey Hinton. 2020. A simple framework for contrastive learning of visual representations. In *Proceedings of the International Conference on Machine Learning (ICML)*.
- [6] Zhuowei Chen, Zhendong Mao, Shancheng Fang, and Bo Hu. 2022. Background Layout Generation and Object Knowledge Transfer for Text-to-Image Generation. In *Proceedings of the ACM International Conference on Multimedia (MM)*.
- [7] Seyone Chithrananda, Gabriel Grand, and Bharath Ramsundar. 2020. Chemberta: Large-scale self-supervised pretraining for molecular property prediction. *arXiv preprint arXiv:2010.09885* (2020).
- [8] Yuntian Deng, Noriyuki Kojima, and Alexander M Rush. 2023. Markup-to-Image Diffusion Models with Scheduled Sampling. In *Proceedings of the International Conference on Learning Representations (ICLR)*.
- [9] Yu Deng, Jiaolong Yang, Dong Chen, Fang Wen, and Xin Tong. 2020. Disentangled and Controllable Face Image Generation via 3D Imitative-Contrastive Learning. In *Proceedings of the IEEE/CVF Conference on Computer Vision and Pattern Recognition (CVPR)*.
- [10] Prafulla Dhariwal and Alexander Nichol. 2021. Diffusion Models Beat GANs on Image Synthesis. In *Proceedings of the International Conference on Advances in Neural Information Processing Systems (NIPS)*.
- [11] Adji Bousso Dieng, Dustin Tran, Rajesh Ranganath, John Paisley, and David Blei. 2017. Variational Inference via χ Upper Bound Minimization. *Proceedings of the International Conference on Advances in Neural Information Processing Systems (NIPS)*.
- [12] Ming Ding, Zhuoyi Yang, Wenyi Hong, Wendi Zheng, Chang Zhou, Da Yin, Junyang Lin, Xu Zou, Zhou Shao, Hongxia Yang, and Jie Tang. 2021. CogView: Mastering Text-to-Image Generation via Transformers. In *Proceedings of the International Conference on Advances in Neural Information Processing Systems (NIPS)*.
- [13] Leo Gao, Stella Biderman, Sid Black, Laurence Golding, Travis Hoppe, Charles Foster, Jason Phang, Horace He, Anish Thite, Noa Nabeshima, et al. 2020. The pile: An 800gb dataset of diverse text for language modeling. *arXiv preprint arXiv:2101.00027* (2020).
- [14] Shanghua Gao, Pan Zhou, Ming-Ming Cheng, and Shuicheng Yan. 2023. Masked Diffusion Transformer is a Strong Image Synthesizer. In *Proceedings of the IEEE/CVF Conference on Computer Vision and Pattern Recognition (CVPR)*.
- [15] Ian Goodfellow, Jean Pouget-Abadie, Mehdi Mirza, Bing Xu, David Warde-Farley, Sherjil Ozair, Aaron Courville, and Yoshua Bengio. 2020. Generative adversarial networks. *Commun. ACM* 63, 11 (2020), 139–144.
- [16] Shuyang Gu, Dong Chen, Jianmin Bao, Fang Wen, Bo Zhang, Dongdong Chen, Lu Yuan, and Baining Guo. 2022. Vector Quantized Diffusion Model for Text-to-Image Synthesis. In *Proceedings of the IEEE/CVF Conference on Computer Vision and Pattern Recognition (CVPR)*.
- [17] Jonathan Ho, Ajay Jain, and Pieter Abbeel. 2020. Denoising Diffusion Probabilistic Models. In *Proceedings of the International Conference on Advances in Neural Information Processing Systems (NIPS)*.
- [18] Zilong Huang, Xinggang Wang, Lichao Huang, Chang Huang, Yunchao Wei, and Wenyu Liu. 2019. Ccnet: Criss-cross attention for semantic segmentation. In *Proceedings of the IEEE/CVF Conference on Computer Vision and Pattern Recognition (CVPR)*.
- [19] Minguk Kang and Jaesik Park. 2020. ContraGAN: Contrastive Learning for Conditional Image Generation. In *Proceedings of the International Conference on Advances in Neural Information Processing Systems (NIPS)*.
- [20] Jingye Li, Hao Fei, Jiang Liu, Shengqiong Wu, Meishan Zhang, Chong Teng, Donghong Ji, and Fei Li. 2022. Unified named entity recognition as word-word relation classification. In *Proceedings of the AAAI Conference on Artificial Intelligence (AAAI)*.
- [21] Ron Litman, Oron Anschel, Shahar Tsiper, Roei Litman, Shai Mazor, and R Manmatha. 2020. Scatter: selective context attentional scene text recognizer. In *Proceedings of the IEEE/CVF Conference on Computer Vision and Pattern Recognition (CVPR)*.
- [22] Nan Liu, Shuang Li, Yilun Du, Antonio Torralba, and Joshua B. Tenenbaum. 2022. Compositional Visual Generation with Composable Diffusion Models. In *Proceedings of the European Conference on Computer Vision (ECCV)*.
- [23] Alexander Quinn Nichol, Prafulla Dhariwal, Aditya Ramesh, Pranav Shyam, Pamela Mishkin, Bob McGrew, Ilya Sutskever, and Mark Chen. 2022. GLIDE: Towards Photorealistic Image Generation and Editing with Text-Guided Diffusion Models. In *Proceedings of the International Conference on Machine Learning (ICML)*.
- [24] Yidong Ouyang, Liyan Xie, and Guang Cheng. 2022. Improving Adversarial Robustness by Contrastive Guided Diffusion Process. *arXiv preprint arXiv:2210.09643* (2022).
- [25] Gaurav Parmar, Dacheng Li, Kwonjoon Lee, and Zhuowen Tu. 2021. Dual Contrastive Generative Autoencoder. In *Proceedings of the IEEE/CVF Conference on Computer Vision and Pattern Recognition (CVPR)*.
- [26] Yanyuan Qiao, Qi Chen, Chaorui Deng, Ning Ding, Yuankai Qi, Mingkui Tan, Xincheng Ren, and Qi Wu. 2021. R-GAN: Exploring Human-like Way for Reasonable Text-to-Image Synthesis via Generative Adversarial Networks. In *Proceedings of the ACM International Conference on Multimedia (MM)*.
- [27] Alec Radford, Jeffrey Wu, Rewon Child, David Luan, Dario Amodei, Ilya Sutskever, et al. 2019. Language models are unsupervised multitask learners. *OpenAI blog* 1, 8 (2019), 9.
- [28] Aditya Ramesh, Prafulla Dhariwal, Alex Nichol, Casey Chu, and Mark Chen. 2022. Hierarchical Text-Conditional Image Generation with CLIP Latents.
- [29] Aditya Ramesh, Mikhail Pavlov, Gabriel Goh, Scott Gray, Chelsea Voss, Alec Radford, Mark Chen, and Ilya Sutskever. 2021. Zero-Shot Text-to-Image Generation. In *Proceedings of the International Conference on Machine Learning (ICML)*.
- [30] Ali Razavi, Aaron Van den Oord, and Oriol Vinyals. 2019. Generating diverse high-fidelity images with vq-vae-2. In *Proceedings of the International Conference on Neural Information Processing Systems (NIPS)*.
- [31] Scott Reed, Zeynep Akata, Xincheng Yan, Lajanugen Logeswaran, Bernt Schiele, and Honglak Lee. 2016. Generative Adversarial Text to Image Synthesis. In *Proceedings of the International Conference on Machine Learning (ICML)*.
- [32] Robin Rombach, Andreas Blattmann, Dominik Lorenz, Patrick Esser, and Björn Ommer. 2022. High-Resolution Image Synthesis with Latent Diffusion Models. In *Proceedings of the IEEE/CVF Conference on Computer Vision and Pattern Recognition (CVPR)*.
- [33] Chitwan Saharia, William Chan, Saurabh Saxena, Lala Li, Jay Whang, Emily L. Denton, Seyed Kamyar Seyed Ghasemipour, Raphael Gontijo Lopes, Burcu Karagol Ayan, Tim Salimans, Jonathan Ho, David J. Fleet, and Mohammad Norouzi. 2022. Photorealistic Text-to-Image Diffusion Models with Deep Language Understanding. In *Proceedings of the International Conference on Advances in Neural Information Processing Systems (NIPS)*.
- [34] Zhenbo Shi, Zhi Chen, Zhenbo Xu, Wei Yang, and Liusheng Huang. 2022. AtHom: Two Divergent Attention Stimulated by Homomorphic Training in Text-to-Image Synthesis. In *Proceedings of the ACM International Conference on Multimedia (MM)*.
- [35] Ming Tao, Hao Tang, Fei Wu, Xiao-Yuan Jing, Bing-Kun Bao, and Changsheng Xu. 2022. Df-gan: A simple and effective baseline for text-to-image synthesis. In *Proceedings of the IEEE/CVF Conference on Computer Vision and Pattern Recognition (CVPR)*.
- [36] Aaron van den Oord, Oriol Vinyals, and Koray Kavukcuoglu. 2017. Neural Discrete Representation Learning. In *Proceedings of the International Conference on Neural Information Processing Systems (NIPS)*.
- [37] Hao Wang, Guosheng Lin, Steven C. H. Hoi, and Chunyan Miao. 2021. Cycle-Consistent Inverse GAN for Text-to-Image Synthesis. In *Proceedings of the ACM International Conference on Multimedia (MM)*.
- [38] Yu Wang, Hengrui Zhang, Zhiwei Liu, Liangwei Yang, and Philip S Yu. 2022. ContrastVAE: Contrastive Variational AutoEncoder for Sequential Recommendation. In *Proceedings of the ACM International Conference on Information & Knowledge Management (CIKM)*.
- [39] Xintian Wu, Hanbin Zhao, Liangli Zheng, Shouhong Ding, and Xi Li. 2022. AdmaGAN: Attribute-Driven Memory Augmented GANs for Text-to-Image Generation. In *Proceedings of the ACM International Conference on Multimedia (MM)*.
- [40] Jiarui Xu, Sifei Liu, Arash Vahdat, Wonmin Byeon, Xiaolong Wang, and Shalini De Mello. 2023. ODISE: Open-Vocabulary Panoptic Segmentation with Text-to-Image Diffusion Models. In *Proceedings of the IEEE/CVF Conference on Computer Vision and Pattern Recognition (CVPR)*.
- [41] Tao Xu, Pengchuan Zhang, Qiuyuan Huang, Han Zhang, Zhe Gan, Xiaolei Huang, and Xiaodong He. 2018. AttnGAN: Fine-Grained Text to Image Generation with Attentional Generative Adversarial Networks. In *Proceedings of the IEEE/CVF Conference on Computer Vision and Pattern Recognition (CVPR)*.
- [42] Hui Ye, Xiulong Yang, Martin Takáč, Rajshekhar Sunderraman, and Shihao Ji. 2021. Improving Text-to-Image Synthesis Using Contrastive Learning. In *British Machine Vision Conference*.
- [43] Han Zhang, Jing Yu Koh, Jason Baldridge, Honglak Lee, and Yinfei Yang. 2021. Cross-modal contrastive learning for text-to-image generation. In *Proceedings of the IEEE/CVF Conference on Computer Vision and Pattern Recognition (CVPR)*.
- [44] Han Zhang, Tao Xu, Hongsheng Li, and et al. 2017. StackGAN: Text to Photorealistic Image Synthesis with Stacked Generative Adversarial Networks. In *Proceedings of the IEEE Conference on Computer Vision (ICCV)*.

- [45] Han Zhang, Tao Xu, Hongsheng Li, Shaoting Zhang, Xiaogang Wang, Xiao lei Huang, and Dimitris N. Metaxas. 2019. StackGAN++: Realistic Image Synthesis with Stacked Generative Adversarial Networks. *IEEE Transactions on Pattern Analysis and Machine Intelligence* 41, 8 (2019), 1947–1962.
- [46] Jing Zhao, Heliang Zheng, Chaoyue Wang, Long Lan, and Wenjing Yang. 2023. MagicFusion: Boosting Text-to-Image Generation Performance by Fusing Diffusion Models. In *Proceedings of the IEEE/CVF Conference on Computer Vision and Pattern Recognition (CVPR)*.
- [47] Yufan Zhou, Bingchen Liu, Yizhe Zhu, Xiao Yang, Changyou Chen, and Jinhui Xu. 2023. Shifted Diffusion for Text-to-image Generation. In *Proceedings of the IEEE/CVF Conference on Computer Vision and Pattern Recognition (CVPR)*.
- [48] Ye Zhu, Yu Wu, Kyle Olszewski, Jian Ren, Sergey Tulyakov, and Yan Yan. 2023. Discrete Contrastive Diffusion for Cross-Modal Music and Image Generation. In *Proceedings of the International Conference on Learning Representations (ICLR)*.

A APPENDIX

A.1 Derivation of ELBO Term

Given the normal sample y_0 , positive sample y'_0 , and the intermediate variables $\{y_t\}_{t=1}^T$ and $\{y'_t\}_{t=1}^T$ from the diffusion process, we present the full derivation of the evidence lower bound of them:

$$\begin{aligned}
\log p(y_0, y'_0) &= \log \int_{y'_1, \dots, y'_{T-1}} \int_{y_1, \dots, y_{T-1}} p(y_0, y_t, y'_0, y'_t) dy_t dy'_t \\
&= \log \mathbb{E}_{q(y_t, y'_t | y_0, y'_0)} \left[\frac{p(y_0, y_t, y'_0, y'_t)}{q(y_t, y'_t | y_0, y'_0)} \right] \\
&\geq \mathbb{E}_{q(y_t, y'_t | y_0, y'_0)} \log \left[\frac{p(y_0, y_t, y'_0, y'_t)}{q(y_t, y'_t | y_0, y'_0)} \right] \\
&= \mathbb{E}_{q(y_t, y'_t | y_0, y'_0)} \log \left[\frac{p(y_0 | y_t) p(y'_0 | y'_t) p(y_t, y'_t)}{q(y_t | y_0) q(y'_t | y'_0)} \right] \\
&= \mathbb{E}_{q(y_t | y_0)} \log [p(y_0 | y_t)] + \mathbb{E}_{q(y'_t | y'_0)} \log [p(y'_0 | y'_t)] \\
&\quad + \mathbb{E}_{q(y_t, y'_t | y_0, y'_0)} \log \left[\frac{p(y_t, y'_t)}{q(y_t | y_0) q(y'_t | y'_0)} \right] \\
&= \mathbb{E}_{q(y_t | y_0)} \log [p(y_0 | y_t)] + \mathbb{E}_{q(y'_t | y'_0)} \log [p(y'_0 | y'_t)] \\
&\quad + \mathbb{E}_{q(y_t, y'_t | y_0, y'_0)} \log \left[\frac{p(y_t, y'_t)}{p(y_t) p(y'_t)} \right] \\
&\quad + \mathbb{E}_{q(y_t, y'_t | y_0, y'_0)} \log \left[\frac{p(y_t) p(y'_t)}{p(y_t | y_0) p(y'_t | y'_0)} \right] \\
&= \mathbb{E}_{q(y_t | y_0)} \log [p(y_0 | y_t)] + \mathbb{E}_{q(y'_t | y'_0)} \log [p(y'_0 | y'_t)] \\
&\quad + \mathbb{E}_{q(y_t, y'_t | y_0, y'_0)} \log \left[\frac{p(y_t, y'_t)}{p(y_t) p(y'_t)} \right] \\
&\quad - D_{KL}[q(y_t | y_0) || p(y_t)] - D_{KL}[q(y'_t | y'_0) || p(y'_t)] \\
&= \mathbb{E}_{q(y_1 | y_0)} \log p(y_0 | y_1) + \mathbb{E}_{q(y'_1 | y'_0)} \log p(y'_0 | y'_1) \\
&\quad - \sum_{t=1}^T D_{KL}(q(y_{t-1} | y_t, y_0) || p(y_{t-1} | y_t)) \\
&\quad - \sum_{t=1}^T D_{KL}(q(y'_{t-1} | y'_t, y'_0) || p(y'_{t-1} | y'_t)) \\
&\quad - D_{KL}[q(y_t | y_0) || p(y_t)] - D_{KL}[q(y'_t | y'_0) || p(y'_t)] \\
&\quad + \mathbb{E}_{q(y_t, y'_t)} \log \left[\frac{p(y_t, y'_t)}{p(y_t) p(y'_t)} \right].
\end{aligned} \tag{15}$$

It is hard to directly solve $\mathbb{E}_{q(y_t, y'_t)} \log \left[\frac{p(y_t, y'_t)}{p(y_t) p(y'_t)} \right]$, and here we assume that $p(y_t, y'_t) = q(y_t, y'_t)$, $p(y_t) = q(y_t)$ and $p(y'_t) = q(y'_t)$

as suggested by [38], then the last term can be written as follows:

$$\begin{aligned}
\log p(y_0, y'_0) &\geq \mathbb{E}_{q(y_1 | y_0)} \log p(y_0 | y_1) + \mathbb{E}_{q(y'_1 | y'_0)} \log p(y'_0 | y'_1) \\
&\quad - \sum_{t=1}^T D_{KL}(q(y_{t-1} | y_t, y_0) || p(y_{t-1} | y_t)) \\
&\quad - \sum_{t=1}^T D_{KL}(q(y'_{t-1} | y'_t, y'_0) || p(y'_{t-1} | y'_t)) \\
&\quad - D_{KL}[q(y_t | y_0) || p(y_t)] - D_{KL}[q(y'_t | y'_0) || p(y'_t)] \\
&\quad + MI(y_t, y'_t)
\end{aligned} \tag{16}$$

A.2 Derivation of EUBO Term

Given the negative sample \bar{y}_0 and the intermediate variables $\{\bar{y}_t\}_{t=1}^T$ from the diffusion process, we present the full derivation of the evidence upper bound of them:

$$\begin{aligned}
\log p(\bar{y}_0) &\leq CUBO_{\chi^2} = \frac{1}{2} \log \mathbb{E}_{q(\bar{y}_t)} \left[\left(\frac{p(\bar{y}_0, \bar{y}_t)}{q(\bar{y}_t)} \right)^2 \right] \\
&\triangleq \exp(2CUBO_{\chi^2}) = \mathbb{E}_{q(\bar{y}_t | \bar{y}_0)} \left[\left(\frac{p(\bar{y}_0, \bar{y}_t)}{q(\bar{y}_t | \bar{y}_0)} \right)^2 \right] \\
&= \mathbb{E}_{q(\bar{y}_{1:T} | \bar{y}_0)} \exp \left[\log \left(\frac{p(\bar{y}_{0:T})}{q(\bar{y}_{1:T} | \bar{y}_0)} \right)^2 \right] \\
&= \mathbb{E}_{q(\bar{y}_{1:T} | \bar{y}_0)} \exp \left[2 \log \frac{p(\bar{y}_{0:T})}{q(\bar{y}_{1:T} | \bar{y}_0)} \right] \\
&= \mathbb{E}_{q(\bar{y}_{1:T} | \bar{y}_0)} \exp \left[2 \log \frac{p(\bar{y}_T) \prod_{t=1}^T p(\bar{y}_{t-1} | \bar{y}_t)}{\prod_{t=1}^T q(\bar{y}_t | \bar{y}_{t-1})} \right] \\
&= \mathbb{E}_{q(\bar{y}_{1:T} | \bar{y}_0)} \exp \left[2 \log \frac{p(\bar{y}_T) p(\bar{y}_0 | \bar{y}_1) \prod_{t=2}^T p(\bar{y}_{t-1} | \bar{y}_t)}{q(\bar{y}_T | \bar{y}_{T-1}) \prod_{t=1}^{T-1} q(\bar{y}_t | \bar{y}_{t-1})} \right] \\
&= \mathbb{E}_{q(\bar{y}_{1:T} | \bar{y}_0)} \exp \left[2 \log \frac{p(\bar{y}_T) p(\bar{y}_0 | \bar{y}_1)}{q(\bar{y}_T | \bar{y}_{T-1})} + 2 \log \prod_{t=1}^{T-1} \frac{p(\bar{y}_t | \bar{y}_{t+1})}{q(\bar{y}_t | \bar{y}_{t-1})} \right] \\
&= \exp \left[\mathbb{E}_{q(\bar{y}_1 | \bar{y}_0)} 2 \log p(\bar{y}_0 | \bar{y}_1) + \mathbb{E}_{q(\bar{y}_{T-1}, \bar{y}_T | \bar{y}_0)} 2 \log \frac{p(\bar{y}_T)}{q(\bar{y}_T | \bar{y}_{T-1})} \right] \\
&\quad + \sum_{t=1}^{T-1} \mathbb{E}_{q(\bar{y}_{1:T} | \bar{y}_0)} \log \frac{p(\bar{y}_T)}{q(\bar{y}_T | \bar{y}_{T-1})} \\
&\quad - \sum_{t=1}^{T-1} \mathbb{E}_{q(\bar{y}_{1:T} | \bar{y}_0)} 2D_{KL}(q(\bar{y}_t | \bar{y}_{t-1}) || p(\bar{y}_t | \bar{y}_{t+1})) \\
&= \exp \left[\mathbb{E}_{q(\bar{y}_1 | \bar{y}_0)} 2 \log p(\bar{y}_0 | \bar{y}_1) \right. \\
&\quad \left. - \mathbb{E}_{q(\bar{y}_{T-1} | \bar{y}_0)} 2D_{KL}(q(\bar{y}_T | \bar{y}_{T-1}) || p(\bar{y}_T)) \right] \\
&= e^{2\mathcal{L}_{elbo}(\bar{y}_0)}.
\end{aligned} \tag{17}$$